

Morphology and evolution of emission line galaxies in the Hubble Ultra Deep Field

N. Pirzkal¹, C. Xu¹, I. Ferreras², S. Malhotra¹, B. Mobasher¹, J. Rhoads¹, A. Pasquali³, N. Panagia¹, A. M. Koekemoer¹, H. C. Ferguson¹, C. Gronwall⁴

ABSTRACT

We investigate the properties and evolution of a sample of galaxies selected to have prominent emission lines in low-resolution grism spectra of the Hubble Ultra Deep Field (HUDF). These objects, eGRAPES, are late type blue galaxies, characterized by small proper sizes ($R_{50} \leq 2kpc$) in the 4350Å rest-frame, low masses ($5 \times 10^9 M_{\odot}$), and a wide range of luminosities and surface brightnesses. The masses, sizes and volume densities of these objects appear to change very little up to a redshift of $z = 1.5$. On the other hand, their surface brightness decreases significantly from $z = 1.5$ to $z = 0$ while their mass-to-light ratio increases two-folds. This could be a sign that most of low redshift eGRAPES have an older stellar population than high redshift eGRAPES and hence that most eGRAPES formed at higher redshifts. The average volume density of eGRAPES is $(1.8 \pm 0.3) \times 10^{-3} h_{70}^3 \text{ Mpc}^{-3}$ between $0.3 < z \leq 1.5$. Many eGRAPES would formally have been classified as Luminous Compact Blue Galaxies (LCBGs) if these had been selected based on small physical size, blue intrinsic color, and high surface brightness, while the remainder of the sample discussed in this paper forms an extension of LCBGs towards fainter luminosities.

Subject headings: galaxies: evolution, galaxies: high redshift, galaxies: formation, galaxies: structure, surveys, cosmology

¹Space Telescope Science Institute, 3700 San Martin Drive, Baltimore, MD21218, USA

²Department of Physics and Astronomy, University College London, Gower Street, London WC1E 6BT

³Institute of Astronomy, ETH Honggerberg, 8093 Zurich, Switzerland

⁴Department of Astronomy & Astrophysics, Pennsylvania State University, 525 Davey Laboratory, University Park, PA 16802

1. Introduction

A majority of nearby galaxies are disk galaxies, still undergoing a significant amount of stellar formation. In order to understand how these objects have evolved towards their current shapes, sizes, and masses, it is important to find out if these objects, as a population, have changed significantly over the last few billions years. Several groups have recently attempted to study disk dominated galaxies over a wide range of redshifts. Ravindranath et al. (2004) observed that disk galaxies, selected from their broad band morphologies did not show a significant sign of size evolution over the redshift range of $0.25 \leq z \leq 1.25$. More recently, Barden et al. (2005) investigated the size evolution of disk galaxies up to $z = 1$ and showed that these luminous objects ($M_v \leq -20.0$) showed a strong evolution in the magnitude-size relation, with an increase in surface brightness of 1 mag per square arc-second in the V band rest-frame. They also found these objects to have lower mass-to-light ratio at $z = 1$ than at the present day and interpreted this as a lack of evolution between stellar mass and effective disk sizes in these objects. Their finding contradicts the results from Ferguson et al. (2004) who found that the size of high redshift ($z \approx 1$ to $z \approx 5$) galaxies appear to evolve as $H^{-1}(z)$, in agreement with hierarchical formation theory. In this paper, we examine the physical properties of a new sample of star-forming galaxies. These objects were selected purely spectroscopically and, unlike previous studies, allow us to examine the morphology, size, surface brightness, and mass evolution of star forming galaxies without having to first pre-assume anything about the physical attributes of these objects. Are higher redshift star forming galaxies smaller, less massive than present day ones? Are their mass-to-light ratio significantly different than present day galaxies? In this paper, we examine these specific issues.

2. Observations

The Hubble Ultra Deep Field (HUDF Beckwith et al. 2005) is currently, and likely to remain for several years, the deepest set of observations ever taken of the sky. The Advanced Camera for Surveys (ACS) images of this field are extremely deep, containing over 10,000-15,000 galaxies down to a limiting magnitude of $z_{850} = 29.5$ (AB magnitude), have a small pixel scale ($0.03''/\text{pixel}$), and a very stable PSF. While the off-axis location of ACS in the HST focal plane results in a significant amount of image distortion, it is now a well calibrated and correctable effect (down to less than 0.1 pixel in the HUDF images). These images thus provide an excellent opportunity to measure the size and morphology of faint galaxies ($M_B \lesssim -18.0$), extending previous studies to much lower luminosities. While the HUDF

images do not provide spectroscopic redshifts of individual sources, the GRAPES program (GRISM ACS Program for Extragalactic Science, PI: Malhotra, see description in Pirzkal et al. 2004) yielded slitless spectroscopic observations of 1400 objects with $i_{775} \leq 27.0$, or about 10% of the sources in the HUDF). We identified 124 objects (eGRAPES) with prominent emission lines (Xu et al. 2005). Ten eGRAPES are Lyman- α sources at $4.1 \leq z \leq 5.8$ (Xu et al. 2005), while the bulk of eGRAPES actually lay at redshifts of $0. \leq z \lesssim 1.5$.

Since the HUDF images reach 2.5 magnitudes deeper than the limiting magnitude of the GRAPES catalog, all of the objects in the GRAPES catalog have very high signal-to-noise images in the B_{435} , V_{606} , i_{775} , and z_{850} HUDF ACS observations (corresponding roughly to the B,V,i, and z bandpasses). We estimate the limiting surface brightness of the HUDF images to be 25.7, 26.5, 25.6, and 24.9 magnitude per square arc-second. In addition to this, near infrared observations of the HUDF have also been available (Thompson et al. 2005) and offer J and H band observations for a large number of these objects, albeit at a much lower resolution (0.09"/pixel). This allows for accurate measurements of the magnitude, shape and size of these objects to be made in different rest-frame wavelengths.

3. Sample and measurements

For the purpose of studying variation in physical properties of eGRAPES as a function of redshift, it is useful to start by defining the following redshift bins, each initially containing an almost equal number of eGRAPES ($\approx 20-30$): $0. \leq z \leq 0.3$, $0.3 \leq z \leq 0.55$, $0.55 \leq z \leq 0.85$, $0.85 \leq z \leq 1.5$. The average (median) redshift of objects in each of these bins is $z = 0.20(0.20), 0.41(0.41), 0.73(0.73), 1.15(1.11)$ respectively. In these four bins, the 4350Å rest-frame corresponds to the observed wavelengths of 5220Å, 6133Å, 7526Å, and 9353Å, nearly equivalent to the B_{435} , V_{606} , i_{775} , z_{850} ACS bandpasses. Throughout this paper, we computed 4350Å rest-frame parameters (magnitude, sizes, morphologies) by linearly interpolating between measurements of these quantities made separately in the two closest available ACS bands.

The initial number of eGRAPES is relatively small (124), but we must further impose a luminosity cut on our sample so that measurements at lower redshifts we make are not biased by less luminous, smaller galaxies whose counterparts would not have been detected at higher redshifts. Assuming a concordant cosmology with $\Omega_M = 0.3, \Omega_\Lambda = 0.7$, and $h = 0.7$, the GRAPES limiting magnitude of $i_{775}=27$ implies that only objects brighter than $M_{B_{435}} \approx -17.5$ would be observed at $z = 1.2$. Based on simulations, we estimate that more than 90% of emission lines with an line equivalent-width greater than 75Å were detected (Xu et al. 2005). Applying this luminosity cut further lowers the number of emission line objects down to 53, and the number of objects remaining in each of our redshift bin is 5, 9, 13, 27.

In this paper, we also carried out a parallel analysis of non-emission line galaxies with known photometric redshifts. The redshifts of these objects were determined by the GOODS project using the combined ACS (BViz) and NICMOS (JH) data from the HUDF and deep K_s band (ISAAC) data. All these data were degraded to the ISAAC seeing (0.4 arcsec) and combined to estimate photometric redshifts by fitting their SEDs to those of rest-frame templates. The photometric redshifts of the non-emission line objects presented in this paper, measured using luminosity function priors, have an accuracy of $(z_{spec} - z_{phot}) / (1 + z_{spec}) \approx 0.08$ (Mobasher et al. 2005). A detailed analysis of these non-emission line galaxies is beyond the scope of this paper and we only use these objects to serve as a comparison sample against which we can compare our eGRAPES sample.

There are several well established methods to measure the size and shape of galaxies and we studied the morphology of eGRAPESs using three separate methods. First, we measured the apparent size (half-light radius, R_{50}) and magnitude each eGRAPES in the B₄₃₅, V₆₀₆, i₇₇₅, and z₈₅₀ bands using the SExtractor program (Bertin & Arnouts 1996) (in dual image mode using a combination of the i₇₇₅ and z₈₅₀ band images as the detection image). Second, we also used the program GALFIT (Peng et al. 2002) to fit a Sérsic profile (Sérsic 1968) to each objects. This profile is of the form $\Sigma(r) = \Sigma_e e^{-k[r/r_e^{1/n} - 1]}$, where r_e is the effective radius of the source, Σ_e is the surface brightness at r_e , n is the power-law index, and $k = k(n)$ is a normalization constant. For $n = 4$, the Sérsic profile reduces to a classic de Vaucouleurs profile while for $n = 1$ it reduces to an exponential disk profile. We used segmentation maps from SExtractor as input masks when running GALFIT and we started each fit with an initial value of $n = 4$. While many eGRAPES appear to be relatively small on the ACS images (≈ 5 HUDF pixels), this did not affect the SExtractor and GALFIT size estimates and both agreed reasonably well.

Third, we computed the Concentration (C) and Asymmetry (A) values (Conselice et al. 2000) of eGRAPESs. Measuring A consists of rotating and subtracting a galaxy image from itself and computing the sum of the absolute value of the residuals. Measuring C consists in computing the logarithm of the ratio of the radii enclosing 20% and 80% of the light in the object. The relations between A, C, and galaxy morphology have been extensively studied in the past (Conselice et al. 2000; Conselice 2003) and have been well calibrated using a sample of nearby objects (Bershady et al. 2000). This last method proved to be the most difficult one to apply to eGRAPES which appear as small objects in the HUDF. Conselice et al. (2000) estimated that a physical image resolution of 0.5 kpc was acceptable in order to produce reliable measurements of A, and they defined the parameter $\epsilon = \frac{\theta_{0.5kpc}}{\theta_{res}}$. As ϵ falls significantly under unity, CAS parameters, and the asymmetry parameter A in particular, become less reliable. Lauger et al. (2004) showed that they were able to successfully measure CAS values of objects with $\epsilon \geq 0.6$. Additionally, the reliability of CAS measurements of

objects with different surface brightnesses was investigated by Lauger et al. (2004). The authors concluded that a signal-to-noise ratio per pixel $\frac{S}{N_{pix}} \geq 1$ was required for unbiased asymmetry measurements (A lower number of high signal-to-noise pixels, as diffuse extended regions of objects become invisible, cause A to be computed using a smaller number of pixels which then artificially increases the estimate of A. See Figure 1 in Lauger et al. (2004)).

The HUDF ACS z band images have a resolution of 0.084" (combining the pixel scale and the size of the ACS PSF), corresponding to $\epsilon \geq 0.7$ for $0 \leq z \leq 6$, which, while lower than the value recommended by Conselice et al. (2000), is larger than the accepted value used by Lauger et al. (2004). We nevertheless independently investigated the effect that small eGRAPES sizes might have on our CAS measurements of these objects. We started by selecting 166 large and bright objects and measured their CAS values after scaling down the size of the images by factors of 2, 3, 4, 5 and 6. We found that A measurements remained robust, and C measurements remained mostly unaffected as long as objects had a half-light radius (R₅₀) that is equal or greater than 5 HUDF pixels. We computed the $\frac{S}{N_{pix}}$ for eGRAPESs in the filter closest to the 4350Å rest frame wavelength and verified that the high-signal to noise ACS imaging ensured that $\frac{S}{N_{pix}} \geq 1$ for these objects.

4. Nature of eGRAPES

Since eGRAPESs were not selected based on their physical attributes, we did not a-priori attempt to select objects with late-type colors and morphologies. One can however distinguish galaxies of different spectral types using a simple rest-frame color versus absolute magnitude plot as well as color versus CAS parameter plots. Bershadsky et al. (2000) showed that determining the spectral type of objects in this manner remains consistent across a broad range of redshifts and angular sizes. Figure 1 shows the eGRAPES population plotted in a rest-frame ($B_{435} - V_{606}$) versus rest-frame $M_{B_{435}}$ magnitude diagram. It is clear from Figure 1 that eGRAPESs are extremely blue compared to local, present day galaxies, and that nearly all eGRAPES are even bluer than local Sc-Irregular galaxies. Figures 2 and 3, confirm that the spectroscopically selected eGRAPESs preferentially occupy the late and intermediate parts of rest-frame ($B_{435} - V_{606}$) versus C and A plots, respectively. In fact, 90% of eGRAPES would be classified as late type if one were to rely on these plots. The high fraction of late-type galaxies amongst eGRAPES has also been confirmed by the work of Mobasher et al. (2005) who assigned irregular or starburst spectral types to 68% of eGRAPES based on photometric band fitting.

4.0.1. Morphology as a function of redshift

We classified eGRAPESs in separate morphological groups based on our Galfit Sérsic fit: mergers ($n < 0.5$), and non-mergers ($n > 0.5$). We assumed that most merger system have in fact light profiles which are significantly flatter than pure exponential profiles (Marleau & Simard 1998). We found that 11 objects with $M_{B_{435}} \leq -17.5$ qualify as mergers (19% of total) and furthermore plot the fraction of merger candidate as a function of redshift in Figure 5. No strong trend is visible in Figure 5 and the fraction of eGRAPES merger candidates remains small at all reshifts except near $z = 1.5$ where the merger fraction increases marginally. The number of available objects is small however and the errors are dominated by small number statistics and a larger population of eGRAPES is required to confirm this observation.

We also computed the asymmetry (A) and concentration (C) of eGRAPESs in the B_{435} rest-frame. As discussed earlier, we restricted the CAS analysis to eGRAPESs that are large enough and that have a surface brightness that is high enough to allow for unbiased CAS measurements. Figure 4 shows that neither the asymmetry nor the concentration of these objects appear to evolve significantly as a function of redshift.

One can only conclude at this point that there does not appear to be a significant change in the average morphology of eGRAPESs, as a population, from the redshift of $z \approx 1.5$ to the present day. However, the number of eGRAPESs for which these measurements could be performed in an unbiased way is small and a much larger sample would be required to definitively state that these objects did not change much, as a population.

5. Size Evolution

We also examine the physical sizes of eGRAPES (half-light radius, R_{50}) as a function of redshift to shed some light on the evolution of this group of star forming galaxies over the last 8 billions years. We computed the apparent B_{435} rest-frame sizes of eGRAPESs (in arc-seconds) by interpolating the half-light radii measured individually using SExtractor in the B_{435} , V_{606} , i_{775} , z_{850} bands. Figure 6 shows the eGRAPES sizes as a function of redshift for objects with $M_{B_{435}} \leq -17.5$, as well as the sizes of photometric redshift galaxies in the field.

Ferguson et al. (2004) showed a sample of what the authors assumed to be disk supported galaxies to be evolving roughly as $\propto H^{-1}$, where H is the Hubble parameter, in agreement with what is expected if the Fall & Efstathiou (1980) model of disk formation with fixed disk circular velocity within dark matter halos is correct. At first glance, it appears that eGRAPES sizes evolve very little as a function of redshift, and certainly less than disk dom-

inated galaxies from previous studies such as (Ferguson et al. 2004). Our control sample of non-emission line, photometric redshift galaxies appear to have sizes that closely follow a $H^{-1}(z)$ evolution model but have sizes that are overall still much smaller than the data from (Ferguson et al. 2004).

Several effects have to be taken into account however before any conclusion can be made. First, eGRAPESs were selected spectroscopically based on the presence of emission lines in their slitless spectra (Pirzkal et al. 2004; Xu et al. 2005). The resolution in such spectra is directly affected by the physical size of the underlying object (Pasquali et al. 2005) which could lead to some biases against the detection of larger objects. As objects get larger, the effective resolution of the grism observations is reduced and the sharpness of any emission line in the spectra is lowered. We estimated this effect using a Monte-Carlo simulation containing 100,000 simulated spectra with a wide range of line equivalent widths, objects sizes and brightnesses. The underlying size distribution of these simulated objects was taken directly from Ferguson et al. (2004) at redshifts of $z = 1.4$ and $z = 2.3$ (with average sizes of $0.6''$ and $0.3''$, respectively). Our simulations showed that most of the emission lines in these simulated spectra, even when they corresponded to objects that were significantly larger than eGRAPESs, were properly detected. The resulting average sizes for the simulated eGRAPESs were $0.5''$ and $0.3''$ in the $z = 1.4$ and $z = 2.3$ bins respectively, hence demonstrating that our eGRAPES sample is not strongly biased towards small sources.

Another thing to keep in mind is that Ferguson et al. (2004) selected objects using a rest-frame UV luminosity cut corresponding to $M_{AB}(1700\text{\AA}) = -21.0$ for a $z \approx 4$ LBG (Steidel et al. 1999), while the small area covered by the HUDF forces us to select objects with $M_{B_{435}} = -17.5$. We did estimate the impact that our luminosity cut has on the average sizes by computing new mean sizes using a series of luminosity cuts: Objects with $0.7L^* \leq L \leq L^*$, where L^* is the luminosity of galaxies with absolute magnitudes M^* , were selected while M^* was varied over a large range of possible values ranging from -23.0 to -16.0 . As increasingly brighter objects were selected using increasingly high luminosity cuts, the average sizes of eGRAPES in each redshift bin increased only marginally (while the number of eGRAPES left in each redshift bin decreased significantly). At $z = 1.15$ (which is within the range of redshifts probed by Ferguson et al. (2004)), the average size of objects increased from $0.2''$ at $M=-16$ to $0.27''$ at $M=-20.5$. The impact of our lower luminosity cut is therefore not likely to be the cause of the large observed size differences shown in Figure 6.

The last thing to realize when comparing eGRAPES sizes to the ones from Ferguson et al. (2004) is that our measurements were made in the B_{435} rest-frame while Ferguson et al. (2004) used the 1500\AA rest-frame. While this has the advantage to allow us to measure the radial extend of these objects based on their global stellar mass distribution rather than based on the instantaneous, unobscured, star formation as measured in the UV (Trujillo et al. 2004), it makes it difficult to compare our results to the Ferguson et al. (2004) results. In

order to properly compare the two, we must estimate the difference in sizes of these objects when observed in the 1500Å and 4350Å rest-frames. We estimated the magnitude of this effect using the sample of galaxies with known photometric redshift from Mobasher et al. (2005) that are at $z \approx 1.9$ and that were successfully detected in the ACS B₄₃₅ band as well as the NICMOS J band observations of the HUDF. Measuring the sizes of these objects in both the B₄₃₅ band and the J band, allowed us to directly measure their sizes in both the 1500Å and 4350Å rest-frames, respectively. Sizes were measured using the same method described above in both the ACS B₄₃₅ band image and the NICMOS J band image. We first matched the resolution of the ACS B₄₃₅ band image to the resolution of the NICMOS image using stars in the HUDF (Pirzkal et al. 2005). We then computed the average ratio of sizes between the degraded ACS B band image (i.e. 1500Å rest-frame) and the NICMOS J band image (i.e. 4350Å rest-frame). We found that the average size ratio is ≈ 0.4 , a value that is somewhat larger than what was observed by Barden et al. (2005) who estimated this bandpass effect to be only 20% at $z \leq 1$, using GEMS galaxies. Figure 7 shows the estimated eGRAPES 4350Å rest-frame sizes compared to the Ferguson et al. (2004) data. By applying this correction to the photometric redshift galaxy sample the size distribution of these objects agree well with the result from Ferguson et al. (2004). On the other hand, eGRAPES remain smaller at all redshifts, even after correction for wavebands.

We compare the size evolution of eGRAPES to that of non-emission line photometric redshift objects by plotting the proper physical size of these objects (in kpc) as a function of redshift, as shown in Figure 8. If sizes increases as $\propto H^{-1}$, one would expect that the proper sizes of these objects to monotonically increase by a factor of 2 between $z = 1.15$ and $z = 0.20$. Such a trend is clearly not present in Figure 8 and no significant evolution (i.e. $> 1\sigma$) is observed. The least square fit of the sizes of eGRAPES is $R_{50}(z) = -0.05 \times z + 1.69$ kpc. The proper sizes of the non star forming galaxies with known photometric redshift are also plotted (dot-dashed line) and show a strong redshift dependence, as expected (Ferguson et al. 2004; Barden et al. 2005). We estimated the effect of cosmological dimming on our size measurements using simulations and one would expect sizes to vary by a factor of two between the reshifts of $z=0.3$ and $z=1.5$, While it is difficult to apply this effect as a correction to our measurements, we can conclude that eGRAPES at low redshifts are certainly no larger than those at higher redshifts and might even have been larger in the past, but this claim would have to be verified with further observations and an larger number of eGRAPES. One is left with the overall picture that eGRAPESs are a population of objects heterogeneous in nature but whose redshift evolution, at least as far as proper sizes are concerned, may not be coupled to the underlying dark matter halo distributions, unlike non-eGRAPES objects. The small field area of the HUDF and the small number of sources does however make this result sensitive to cosmic variation and small number statistics. Further HST/ACS grism

observations, over a wider area, such as from the PEARS project (Probing Evolution And Reionization Spectroscopically, PI: Malhotra) should allow us to confirm this result in the future.

Related to the size evolution of eGRAPES, is the question of surface brightness evolution of these objects. Following Barden et al. (2005), we can compute the effective surface brightness of these objects in the rest-frame B band using:

$$\mu_B = M_b + 5 \log R_e + 2.5 \log q + 38.568, \quad (1)$$

where M_b is the absolute rest-frame magnitude in the B-band, R_e is the half-light radius in kpc from our GALFIT fits, and q is the axis ratio of the object determined by GALFIT. We computed the effective surface brightness of eGRAPES and photometric redshift galaxies and plot it as a function of redshift in Figure 9. A strong monotonic decrease in the surface brightness (≈ 2.5 magnitudes) is visible between the redshift of $z=1.15$ to $z=0.2$. The same effect is however observed in the non-emission line objects in the field, albeit the later have on average a much lower surface brightness than eGRAPES (by about ≈ 1 mag at all redshifts). The surface brightness evolution of eGRAPES does not therefore appear to be peculiar and the only distinction that eGRAPES have when compared to other galaxies in the field is that they have a very high surface brightness. Figure 9 also shows the effect that cosmological dimming has on the measured effective surface brightness. The change in effective surface brightness caused by surface dimming is essentially flat, especially from $z=0.5$ to $z=1.5$, with a decrease of 0.6 magnitude from $z=0.25$ to $z=1.5$. Simulations showed that as objects were dimmed artificially, the measured radius decreased while the measured object flux also decreased, causing the surface brightness to remain mostly unaffected. These simulations were done by taking low redshift eGRAPES, scaling down the flux originating from the source (after masking out the background regions of the image), re-computing and adding poisson noise to the dimmed down image, adding back the original background, and re-running SExtractor and GALFIT to derived new sizes for the object.

6. Size-color and Size-luminosity relations

The effective surface brightness of eGRAPES increases with redshift, which could potentially be an indication of a change in the average stellar population of eGRAPES as a function of redshift. It is interesting to actually examine whether the size of eGRAPES is related to their stellar population. Figure 10 shows eGRAPES plotted in a rest-frame (B-V) vs R_{50} plot. As this figure shows, there does not appear to be a correlation between the two. We found that eGRAPES have a median size of 1.28 kpc with sizes ranging from

$0.1 \leq R_{50} \leq 3.1$ kpc, and a median luminosity of $M_{4350\text{\AA}}^{\circ} = -19.8$. Figure 11 further shows how the size and luminosity of eGRAPES compare to local galaxies and to $z \approx 3.0$ objects from the Hubble Deep Field (UDF) (Lowenthal et al. 1997, and reference therein). We find that eGRAPESs are significantly smaller and less luminous than the bulk of elliptical galaxies and slightly smaller than most of the $z \approx 3$ sources identified in the HUDF. On the other hand, eGRAPES sizes are consistent with the observed sizes of local irregulars, dwarfs, HII and CNELGs (Compact Narrow Emission Line Galaxies). Yet, eGRAPESs appear to be significantly less luminous than local irregulars at any given size, or, equivalently, have significantly smaller sizes at any given luminosity than local irregulars, resulting in eGRAPESs appearing as objects with high surface brightness as shown in Figure 9.

7. Mass Estimates

We can further investigate the nature of eGRAPES by computing estimates of their mass-to-light ratios and masses. These estimates were conducted using two independent techniques. First, we used the method of Bell et al. (2003), as used by Barden et al. (2005), which relates the rest-frame color of galaxies to their SDSS r-band mass-to-light ratio and which, when using the rest-frame (B-r) color was shown to be relatively insensitive to the detailed star formation history, metallicity, and dust content of galaxies. We computed the rest-frame (B-r) colors of eGRAPES as described above. The presence of emission line in the spectra of these objects was taken into account and results in at most a 0.05–0.10 magnitude photometric uncertainty which in turn corresponds to an error in the mass estimates of these objects of about 20%. The mass estimates obtained in this manner are somewhat uncertain ($\approx 10 - 30\%$), especially for late-type objects such as eGRAPES. The results we discuss in this paper are for a population of star-forming galaxy as a whole and not for individual objects. We cannot of course follow the evolution of any single star-forming galaxy. What we can do however is to examine whether the entire population of eGRAPES has changed during the past few billions years.

The mass of eGRAPES, \mathcal{M} , allowing for the differences between the SDSS and the ACS filters (Fukugita et al. 1995), can be estimated using:

$$\log \mathcal{M}/L_r = -0.706 + 1.152 \times (B_{435} - V_{606}), \quad (2)$$

and the stellar mass of

$$\log \mathcal{M} = \log \mathcal{M}/L_r - 0.4 \times (r_s - 5 \log D_L - 29.67), \quad (3)$$

where r_s is the apparent Sérsic magnitude at 6250\AA , and D_L is the luminosity distance of the object.

The second method we used is significantly more involved and involves the modeling of the stellar populations of each object separately in order to determine its mass-to-light ratio from the data. We followed a phenomenological approach describing the star formation history by a reduced set of parameters, which allowed us to scan a large range of possible star formation histories using a two stellar component system (Ferrerias & Silk 2000). Each of these component is a simple stellar population from the models of Bruzual & Charlot (2003), with a Salpeter IMF in the standard mass range ($0.1 - 100M_\odot$). We assumed the same metallicity for both components, and we included the effect of dust reddening and attenuation from the prescription of Charlot & Fall (2000) for the younger component.

The parameters that describe this model are the ages of both components (t_Y and t_O); the mass ratio between the components (e.g. characterized by f_Y , the mass fraction in young stars); and the metallicity of both populations and the dust content – given by $E(B - V)$. We chose three different metallicities: $Z/Z_\odot = \{1/10, 1/3, 1\}$ and explored a grid of $16 \times 16 \times 16 \times 16$ star formation histories for each metallicity, which comprises the range of parameters shown in Table 1. We used B_{435} , V_{606} , i_{775} , and z_{850} photometry from the ACS images and – where available (86 out of 114 objects) – NICMOS J and H photometry. We did not allow the eGRAPES redshifts to change and, for each galaxy, the grid of models described above was run and a maximum likelihood method was used to determine the stellar masses. Figure 12 shows the derived masses for each choice of metallicity, as well as the masses obtained using the simple photometric method described earlier. We have not included the error bars for the uncertainties expected from the color-SFH degeneracy, which amount to ~ 0.3 dex in $\log M/M_\odot$.

Based on the fact that the eGRAPES sample selection was limited to objects with $i_{775} < 27$, we can estimate the lower limiting stellar mass of the eGRAPES sample by assuming a typical stellar population for these galaxies. Assuming an age of 0.5 Gyr, we find that the limiting eGRAPES stellar mass is $\log M/M_\odot \sim 7.6(8.5)$ at $z = 0.5(1)$. This is well below the eGRAPES SED derived mass estimates shown in Figure 12. Figure 12 shows the individual and binned eGRAPES photometric mass estimates as well as the binned averages of the SED derived masses computed for 1/10, 1/3, and solar metallicities. The average photometric-mass of the eGRAPES population is $(4.5 \pm 2.1) \times 10^9 M_\odot$. Our SED-fitting method yielded the mass estimates of $5.1 \pm 3.5 \times 10^9 M_\odot$, $2.4 \pm 0.5 \times 10^9 M_\odot$, and $2.4 \pm 0.5 \times 10^9 M_\odot$ for assuming solar, 1/3 solar, and 1/10 solar metallicities, respectively. All of our mass estimates agree well and are essentially redshift independent. We find that eGRAPESs have masses that are similar to that of low-mass galaxies (e.g. $\leq 10^{10} M_\odot$) and about 10 times lower

than L^* galaxies today (Guzmán et al. 1996), independently of the metallicity we assumed for these objects. eGRAPES masses are similar to the mass estimates of Compact Narrow Emission Line Galaxies (CNELG) and luminous compact blue galaxies (LBG) ($5 \times 10^9 M_\odot$, Guzmán et al. 1996). These objects, which are believed to be star forming galaxies, are believed by some to be the progenitors of today’s more massive spiral disk galaxies (Phillips et al. 1997) or local dwarf elliptical galaxies (Guzmán et al. 1996, 1997, 1998). The relation between eGRAPESs and LCBGs is discussed further in the next section.

Figure 13 further shows the estimated mass-to-light ratio of the eGRAPES sample. The mass-to-light ratio of these objects is low (≤ 1.0), indicating that eGRAPES are objects with a young stellar population and/or that have just undergone some major starburst. Figure 13 also indicates that the mass-to-light ratio of eGRAPES is lower at high redshifts. While we observed most of the physical attributes (such as sizes and morphology) of eGRAPES to be uncorrelated to redshift, the increase in mass-to-light ratio at lower redshift could be due to the fact that, on average, the observed stellar population of eGRAPES is older at lower redshifts. This could be evidence that, on average, eGRAPES were more actively forming stars at higher redshifts, or that, alternatively, that we observe more newly born eGRAPES at high redshifts, assuming that younger galaxies have a higher fraction of mass in the form of gas and therefore a higher star formation rate per unit mass).

A possible alternative would be that eGRAPES are more luminous at higher redshifts, even though they are observed to have similar sizes at all redshifts. However, while we do observe a lower number of high luminosity eGRAPES ($M_{B_{435}} \leq -20.0$) at low redshifts than at high redshifts, one must keep in mind that the HUDF field is small and that the volumes probed at low redshifts are small. The change of observing high luminosity eGRAPES at low redshifts is therefore low. For example, if we restrict ourselves to [OII] emission line eGRAPES at a redshift $0.3 \leq z \leq 1.3$ with $M_{B_{435}} \leq -17.5$, we find that $60 \pm 14\%$ eGRAPES have $M_{B_{435}} \leq -20.0$ at $0.8 \leq z \leq 1.3$ while $41 \pm 15\%$ eGRAPES have $M_{B_{435}} \leq -20.0$ at $0.3 \leq z \leq 0.8$. An increase in the number of high luminosity eGRAPES as a function of redshift is therefore not significantly detected in this study and the difference in the number of observed bright eGRAPES can be explained away as the result of the relatively small volume that is probed by this study at low redshifts. It is therefore likely that the observed redshift dependence of the eGRAPES mass-to-light ratio is the result of genuinely different stellar populations.

8. Nature of eGRAPES: Luminous compact blue galaxies?

We found eGRAPES to be emission line galaxies that are intrinsically very blue, compact galaxies of only a few kpc in size, and with a high surface brightness. These objects are reminiscent of a class of objects called luminous compact blue galaxies (LCBG, Garland et al. 2004, 2005). These were initially identified as very blue, unresolved stellar sources in ground based QSO surveys (Koo et al. 1994). LCBGs have since been shown to be a somewhat heterogeneous group of objects composed of small star forming galaxies undergoing vigorous star formation. The exact definition of LCBGs is somewhat loosely defined and currently being refined by Jangreen et al. (2005). They include compact narrow emission line galaxies (CNELGs) (Koo et al. 1994, 1995; Guzmán et al. 1996; Phillips et al. 1997; Guzmán et al. 1998) and blue nucleated galaxies at larger redshifts (Schade et al. 1995, 1996). Based on the work from Guzmán et al. (2003); Werk et al. (2004); Jangreen et al. (2005), we can identify LCBG candidates amongst the eGRAPES sample by selecting eGRAPES that have a high surface brightness ($SB_e \leq 21.0 \text{ mag arcsec}^{-2}$), are blue ($B - V < 0.6$), and have a high luminosity ($M_B \leq -18.5$). While eGRAPES were not initially selected based on these size, surface brightness, and luminosity cuts, Figure 14 shows that LCBGs appear to be a natural sub-group of the eGRAPES sample. We find that approximately 60% of eGRAPES satisfy the Werk et al. (2004) LCBG selection criteria. In Figure 14, the very bright object at $M_B < -25$ is likely to be a quasar and was detected in the X-ray by Koekemoer et al. (2004), while the spectra of the four objects with $\mu_B \leq 12$ show these objects to be a faint QSO and three unobscured (Type 1) AGNs whose GRAPES spectra show [OIII] emission with high equivalent width.

The average volume density of eGRAPES ($M_{B_{435}} \leq -17.5$) is $(1.8 \pm 0.3) \times 10^{-3} h_{70}^3 \text{ Mpc}^{-3}$ between $0.3 < z \leq 1.5$. The volume densities of the eGRAPES LCBG candidates over the same redshift range is $(1.6 \pm 0.2) \times 10^{-3} h_{70}^3 \text{ Mpc}^{-3}$ while they are $(2.0 \pm 0.7) \times 10^{-3} h_{70}^3 \text{ Mpc}^{-3}$ and $(2.5 \pm 0.6) \times 10^{-2} h_{70}^3 \text{ Mpc}^{-3}$ for objects at $0.4 \leq z \leq 0.7$ and $0.7 \leq z \leq 1.0$ respectively. Phillips et al. (1997) estimated the LCBG volume densities to be $2.2 \times 10^{-3} h_{75}^3 \text{ Mpc}^{-3}$ and $8.8 \times 10^{-3} h_{75}^3 \text{ Mpc}^{-3}$ at $0.4 < z < 0.7$ and $0.7 < z < 1.0$, respectively, an increase by a factor of four from low to high redshifts. If we restrict the sample of eGRAPES LCBG candidates to objects with $M_B \leq -18.5$ the computed densities become $1.5 \times 10^{-3} h_{70}^3 \text{ Mpc}^{-3}$ and $1.8 \times 10^{-3} h_{70}^3 \text{ Mpc}^{-3}$ for $0.4 < z < 0.7$ and $0.7 < z < 1.0$, respectively. More recently, Werk et al. (2004) found the density of local ($z < 0.045$) LCBGs to be $5.4 \times 10^{-4} h_{70}^3 \text{ Mpc}^{-3}$. We do not however detect a large increase in LCBG volume density as a function of redshift but the HUDF field is however small and the numbers of eGRAPES LCBG candidates in each bins are small (6 and 12).

9. Conclusion

The GRAPES survey has allowed us to select emission line galaxies, eGRAPES, without having to first pre-select objects based on their apparent size, luminosity, or surface brightness. We found that our spectroscopic selection method allowed us to efficiently select a significant population of star-forming, late type galaxies over a wide range of redshifts. We observe these objects to be very blue (Rest-frame $(B - V) \lesssim 0.55$), to have a high surface brightness (≈ 1 magnitude brighter than non emission line objects in the field), small physical sizes ($\approx 1 - 2$ kpc), and relatively small masses ($\approx 5 \times 10^9 M_\odot$). We did not find any strong correlation between the eGRAPES intrinsic color and sizes. We did observe the surface brightness of eGRAPES to increase significantly as a function of redshift (≈ 2 magnitudes between $z=0.2$ and $z=1.15$), but found no evidence that the size of eGRAPES change with redshifts. The mass-to-light ratio of these objects decreases as a function of redshift by an amount that is consistent with the observed increase in surface brightness (≈ 2.5 from $z=0.2$ to $z=1.15$). This is evidence that, on average, eGRAPES were more actively forming stars at higher redshifts, or that, alternatively, that we observe more newly born eGRAPES at high redshifts. This could be evidence that most eGRAPES have formed at higher redshifts. We observed that eGRAPES, while sharing many characteristics of LCBGs and CNELGs, spanned a much wider range of luminosities (reaching down to much lower luminosities). While the number of eGRAPES LCBG is small, we did not find a strong redshift dependence of the volume density of these objects.

This work was supported by grant GO-09793.01-A from the Space Telescope Science Institute, which is operated by AURA under NASA contract NAS5-26555.

Table 1. Summary of the parameters used to model the stellar populations of each eGRAPES separately, as described in Section 7.

| | |
|---|------------------------------|
| Age of young component, $\log(t_Y)$ (Gyr) | -3.0...-1.0 |
| Age of old component, t_O (Gyr) | 0.5... $t_u(z)$ ¹ |
| Mass fraction in young stars, f_Y | 0.0...1.0 |
| Dust (young component), E(B-V) (mag) | 0.0...2.0 |

¹ $t_u(z)$ is the age of the Universe at the redshift of the galaxy. A Λ CDM concordance cosmology is adopted.

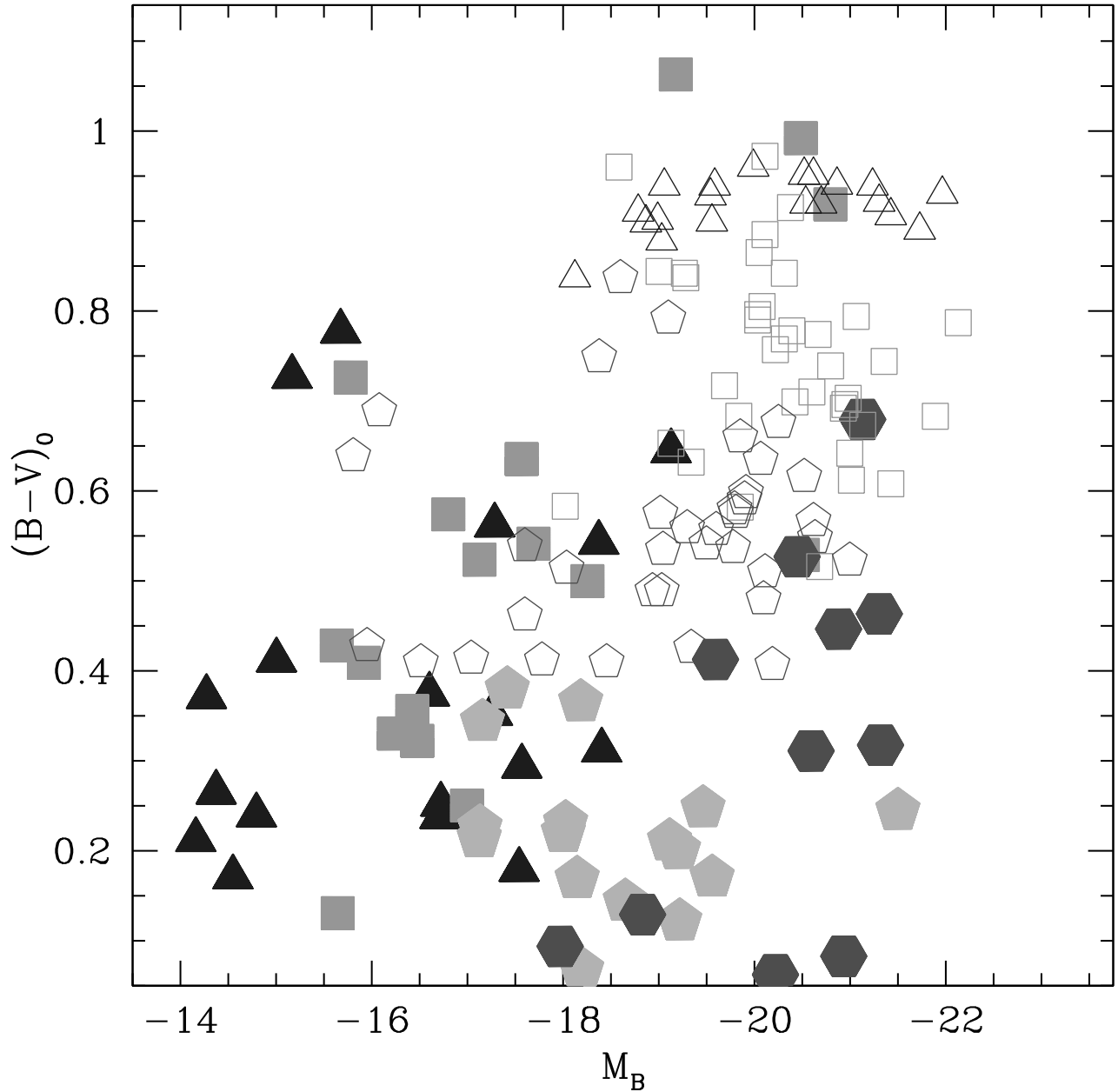


Fig. 1.— Rest-frame $(B_{435} - V_{606})$ vs rest-frame $M_{B_{435}}$. The empty symbols are low redshift galaxies from Bershady et al. (2000), Frei et al. (1996), and Kent (1984). E-S0, Sa-Sb, and Sc-Irr are shown using triangles, squares, and pentagons, respectively. The solid symbols represent eGRAPES objects. eGRAPES at $0 < z \leq 0.3$, $0.3 \leq z \leq 0.55$, $0.55 \leq z \leq 0.85$, and $0.85 \leq z \leq 1.5$ using triangles, squares, pentagons, and hexagons, respectively. Most eGRAPES have bluer rest-frame colors and lower luminosities than even the local Sc-Irr objects shown in Bershady et al. (2000).

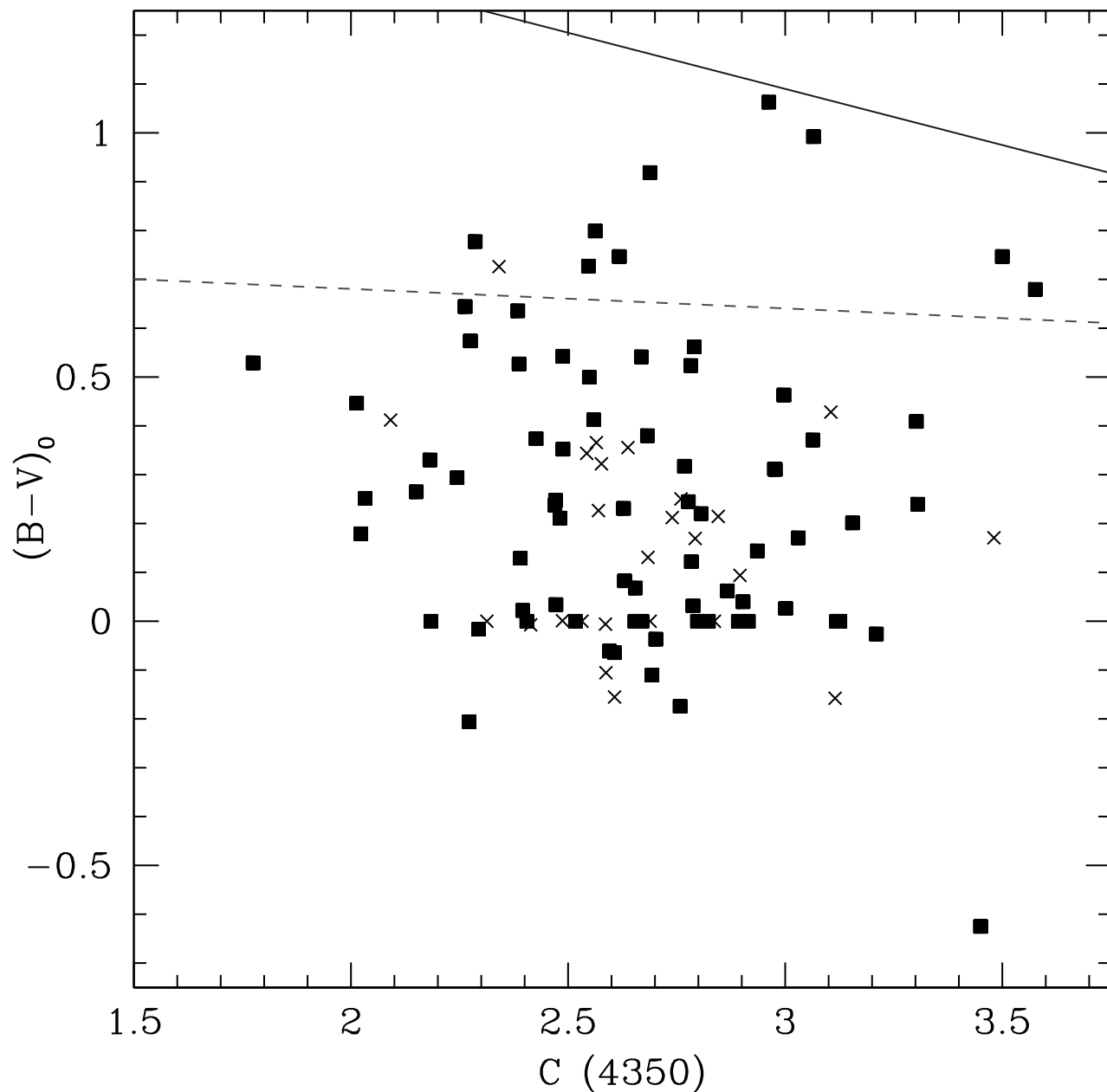


Fig. 2.— Rest-frame $(B_{435} - V_{606})$ vs Concentration for eGRAPES. Late type objects are in the region under the dash curve. Early type objects are above the solid curve. Intermediate objects are between the two curves (Bershady et al. 2000). The crosses are objects with marginal surface brightness and/or that are smaller than 5 HUDF pixels and for which CAS values might be suspect. 90% of eGRAPES are late type galaxies.

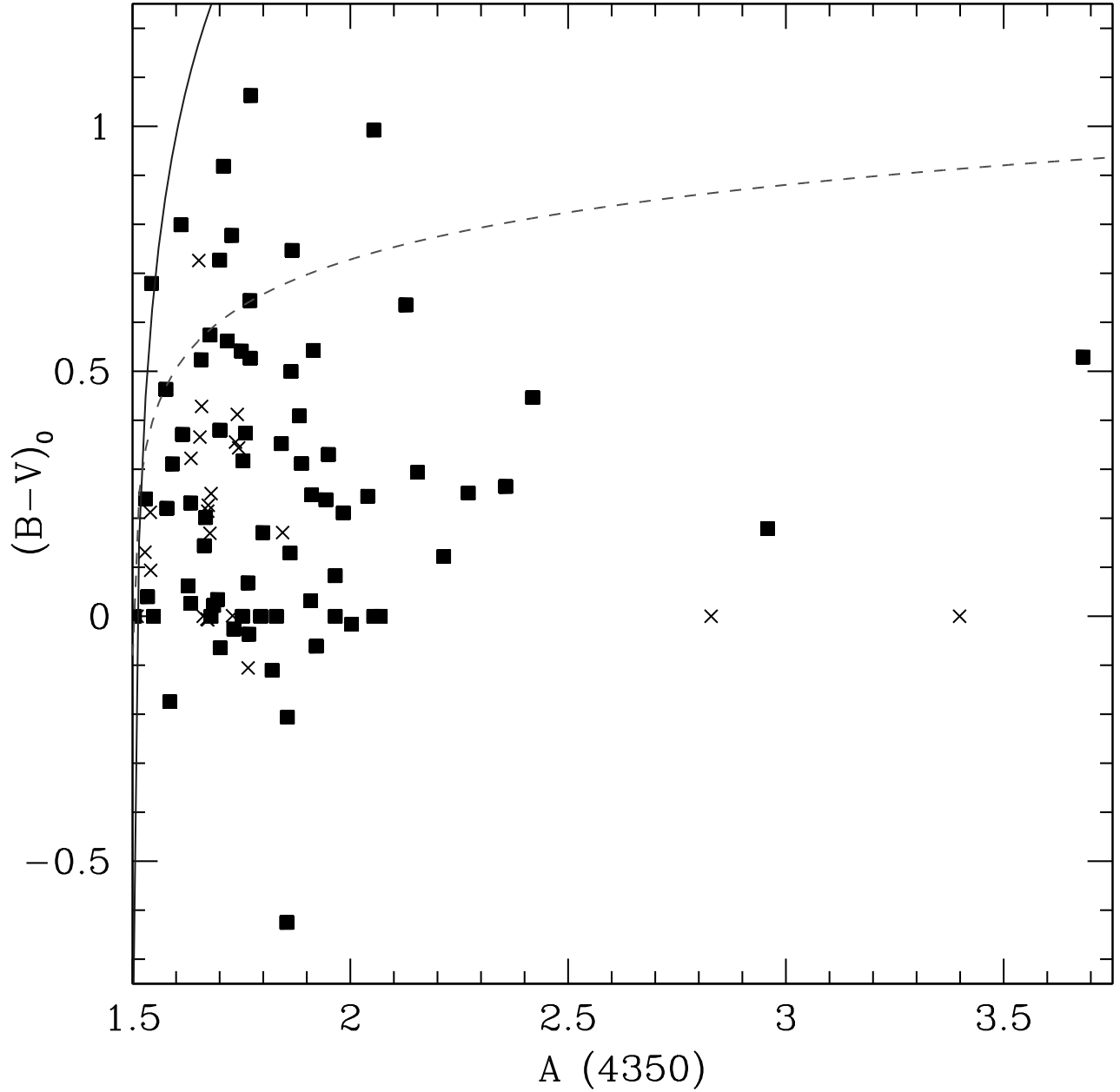


Fig. 3.— Rest-frame $(B_{435} - V_{606})$ vs Asymmetry. Late type objects are in the region under the dash curve. Early type objects are above the solid curve. Intermediate objects are between the two curves (Bershady et al. 2000). The crosses are objects with marginal surface brightness and/or that are smaller than 5 HUDF pixels and for which CAS values might be suspect.

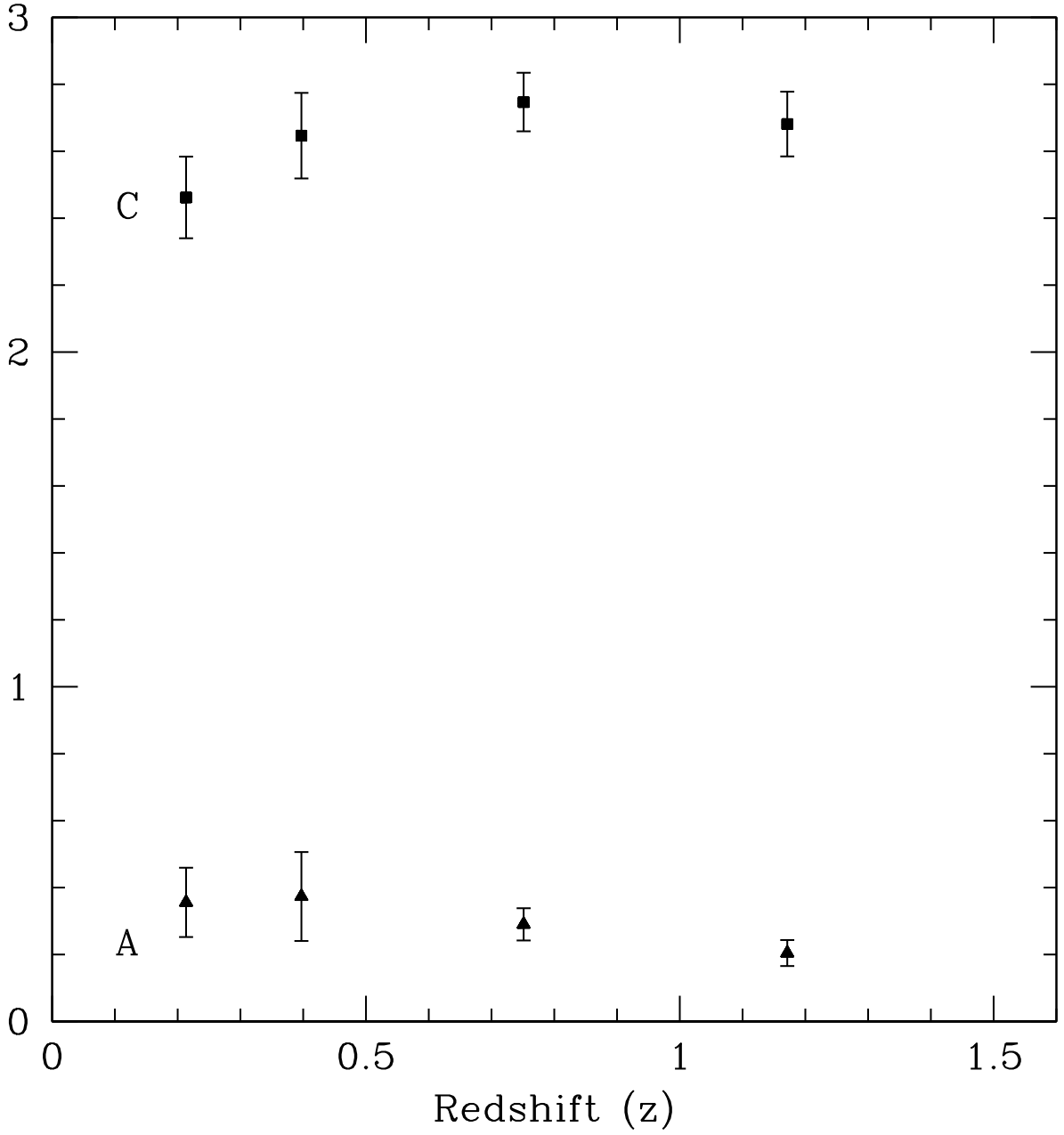


Fig. 4.— 4350Å rest-frame asymmetry (A, bottom points) and concentration (C, top points) values for eGRAPES with $M_{B_{435}} \leq -17.5$. These are the values averaged in each of redshift bins, and the error bars are the standard deviation of the mean. Neither the asymmetry nor the concentration of eGRAPESs vary significantly from $z \approx 1.5$ to the present day.

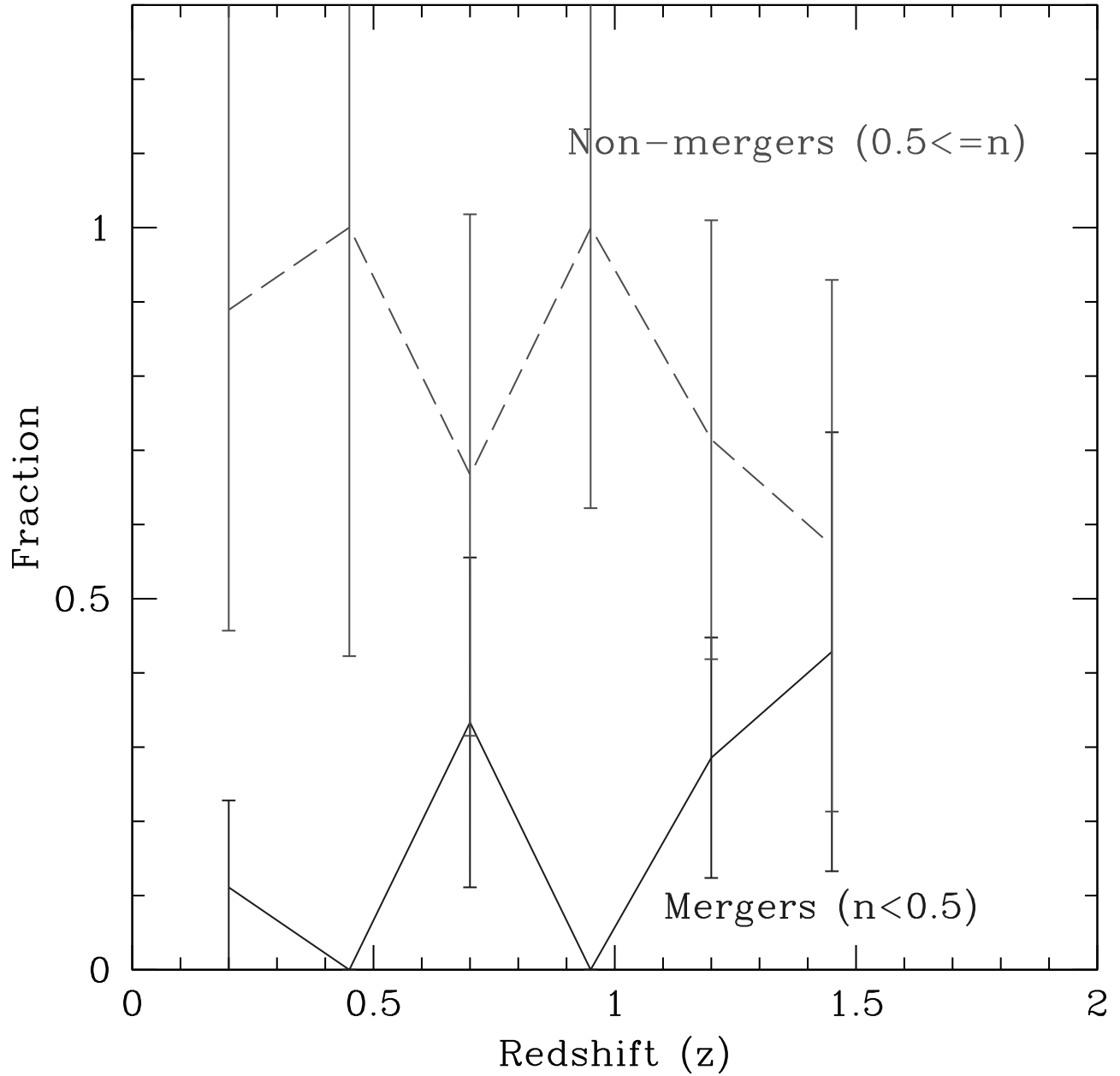


Fig. 5.— Redshift evolution of the ratio of merger, and non-merger eGRAPES to the total number of eGRAPES, as a function of redshift. Only objects with $M_{B_{435}} \leq -17.5$ are included. eGRAPES best fitted by a Sérsic index smaller than 0.5 are classified as mergers. The large error bars (1σ) reflect the small number of available sources. The overall fraction of mergers (i.e. significantly flatter profiles than exponential profiles) is small at all redshifts and does not appear to vary significantly as a function of redshift.

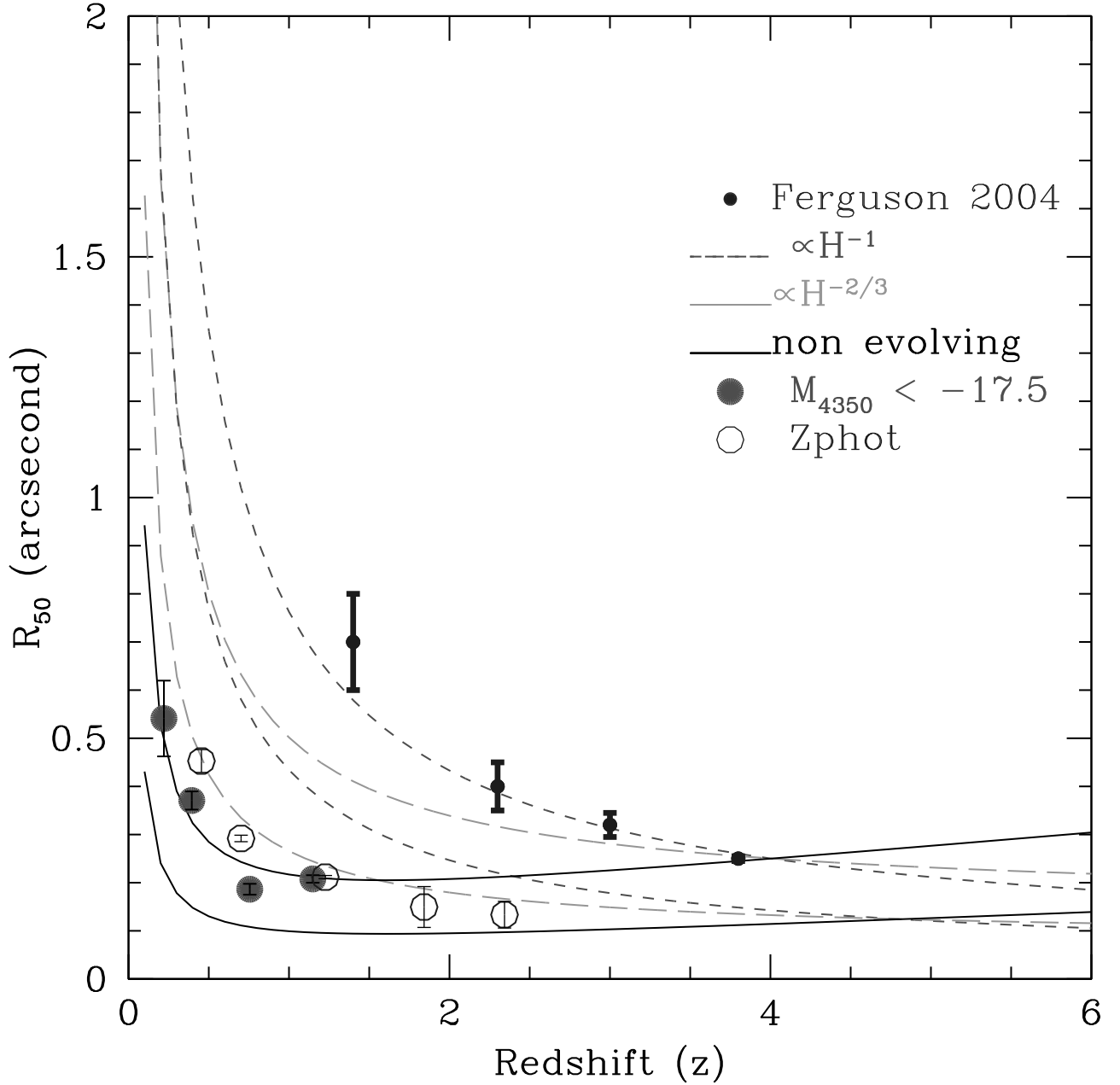


Fig. 6.— Measured, apparent sizes (in ") of eGRAPES in the 4350Å rest-frame as a function of redshift. eGRAPES are plotted in large filled circles. The sizes of Ferguson et al. (2004) disk galaxies are plotted in small solid circles. The error bars we show for the eGRAPES points are the 95% confidence limit of our measurements. The errors bars from the Ferguson et al. (2004) data are their original error bars which were determined using simulations. The solid lines show the expected size distribution in the case of non-evolution. The long dash and short dash curves are as in Ferguson et al. (2004) and show the expected evolution if sizes scaled as the halo masses ($R \propto H^{-1}(z)$ for disks with fixed circular velocity (red) or $R \propto H^{-2/3}(z)$ for fixed mass (green)). The various evolution models are shown using two different normalization at $z = 4$.

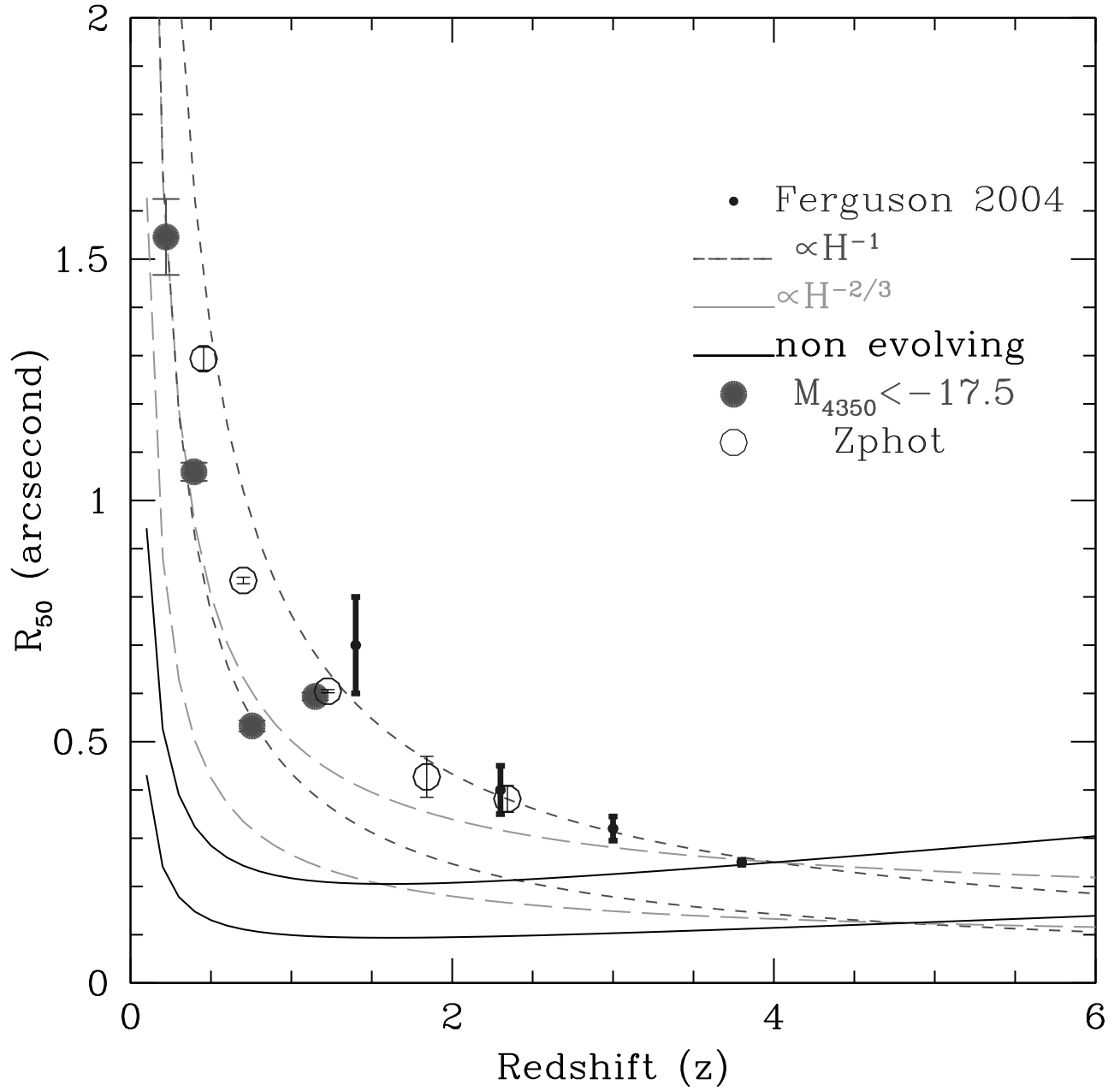


Fig. 7.— Estimated, apparent sizes (in ") of eGRAPES in the 1500\AA rest-frame as a function of redshift. eGRAPES are plotted in large filled circles. Symbols and lines are as in Figure 6..

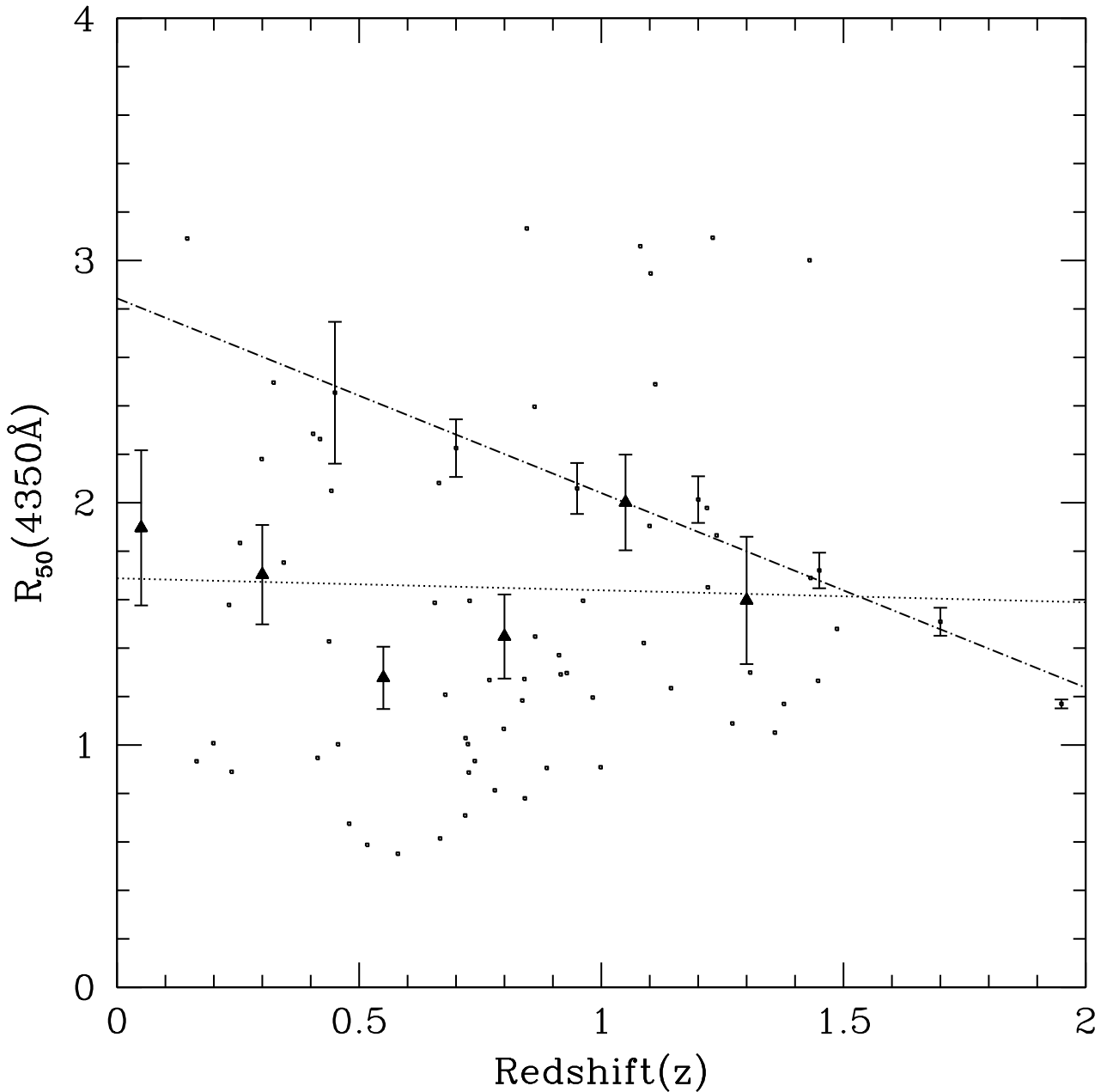


Fig. 8.— Physical size (in kpc) of the $M_{B_{435}} \leq -17.5$ eGRAPES in the B_{435} rest-frame. The sizes of non emission line, photometric redshift galaxies are also shown (dot-dash line) for comparison. Compared to non emission line galaxies, eGRAPES are observed to have a much more heterogeneous distribution of sizes and show little evidence of a strong redshift-size relation. The dot-dashed lines show the least square fits to the sizes of eGRAPES and photometric redshift galaxies. Errors bars are the standard deviation in each of the chosen redshift bins.

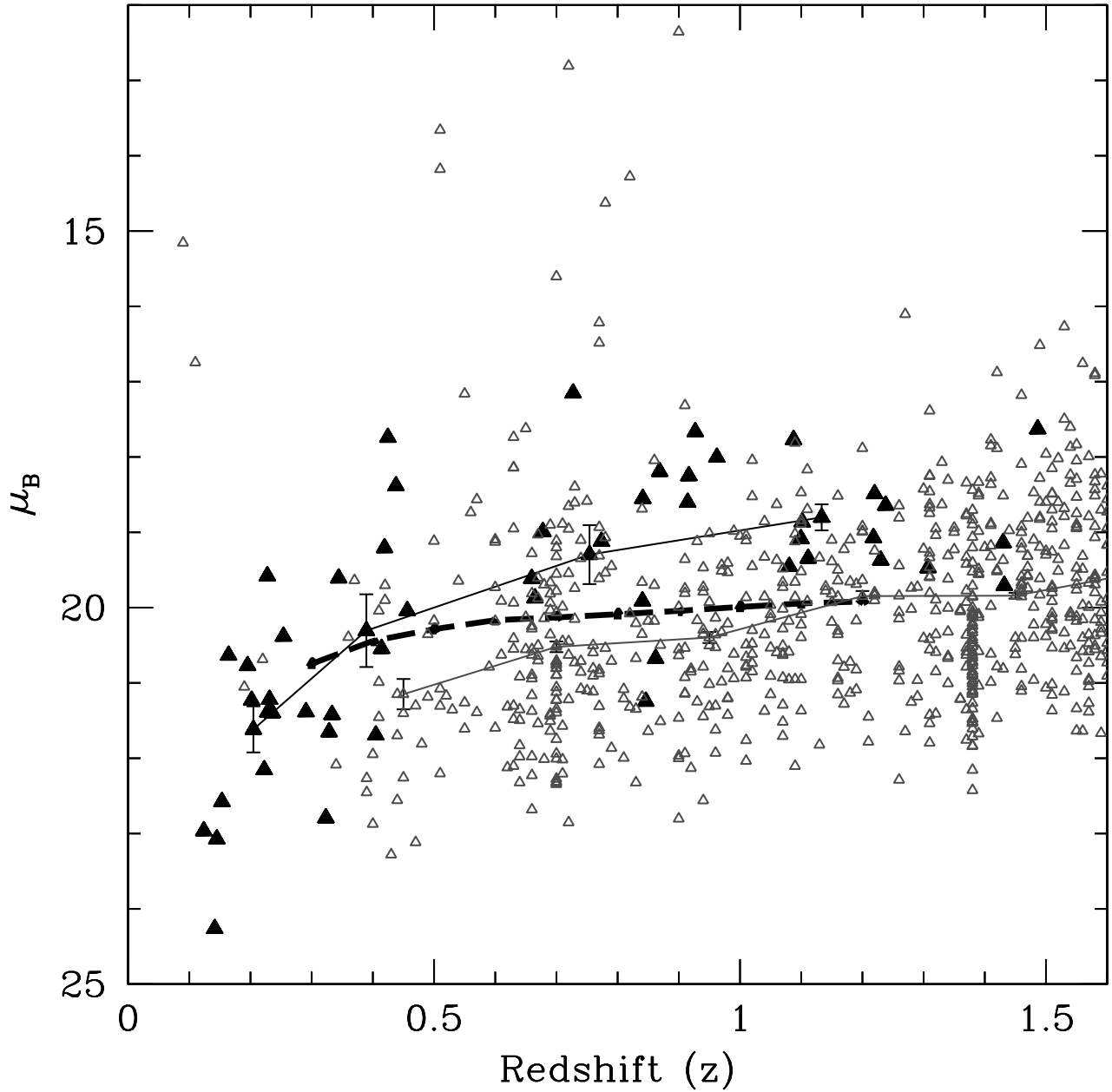


Fig. 9.— Surface brightness of eGRAPES (solid triangles) and non emission line photometric redshift galaxies (open triangles) as a function of redshift. Average values at redshifts of $z = 0.20, 0.41, 0.73, 1.15$ are also shown. The mean surface brightness is observed to decrease by ≈ 2.0 magnitudes per arc-second² from $z=1.15$ to $z=0.2$. The dash line shows the simulated effect of cosmological dimming on effective surface brightness measurements. The observed changes in surface brightness as a function of redshift is stronger than the simulations.

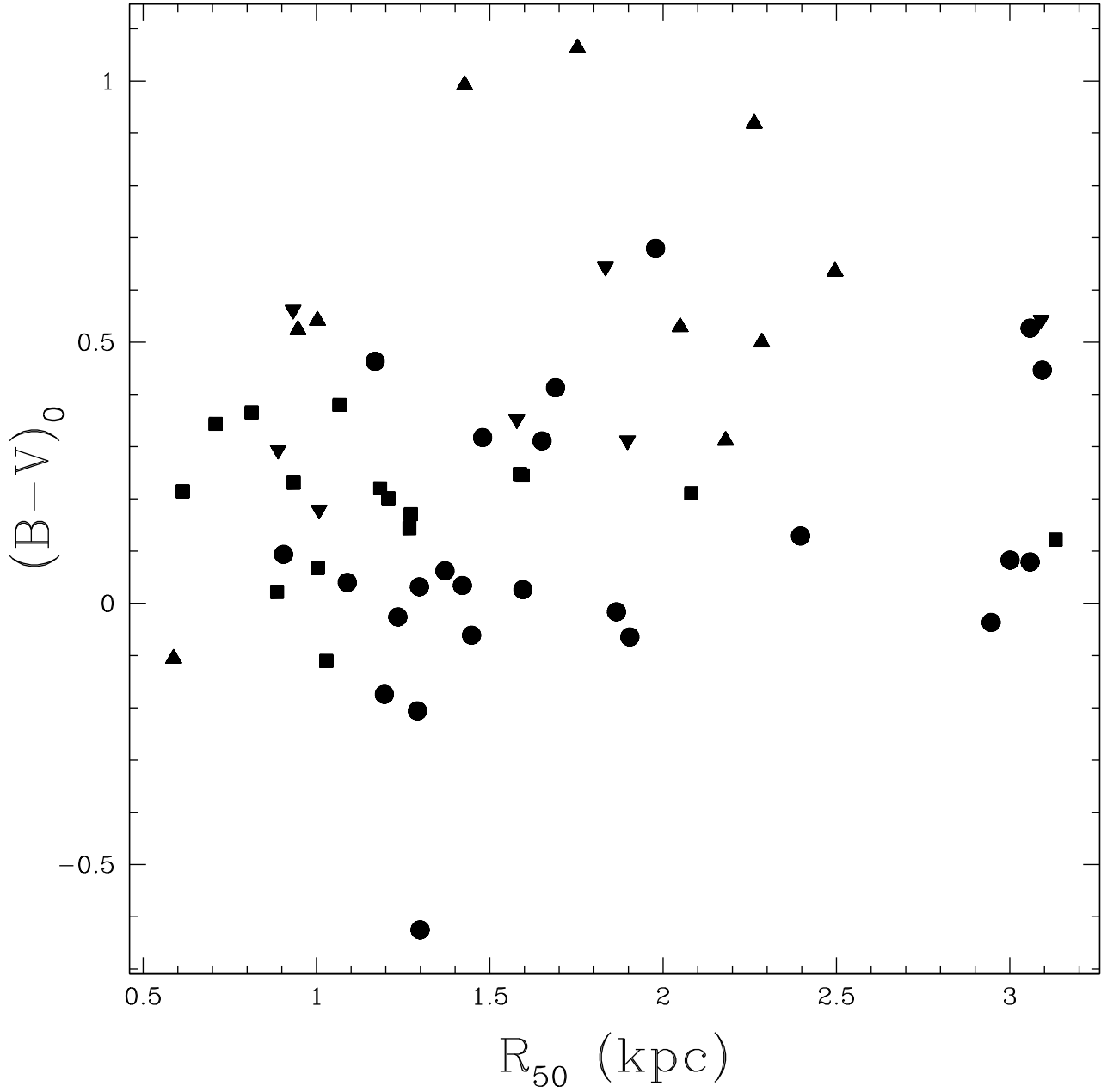


Fig. 10.— Physical sizes and rest-frame $(V_{606} - V_{606})$ colors of eGRAPES. The filled inverted triangles, triangles, squares, and circles are objects at $0 \leq z \leq 0.3$, $0.3 \leq z \leq 0.55$, $0.55 \leq z \leq 0.85$, $0.85 \leq z \leq 1.5$, respectively.

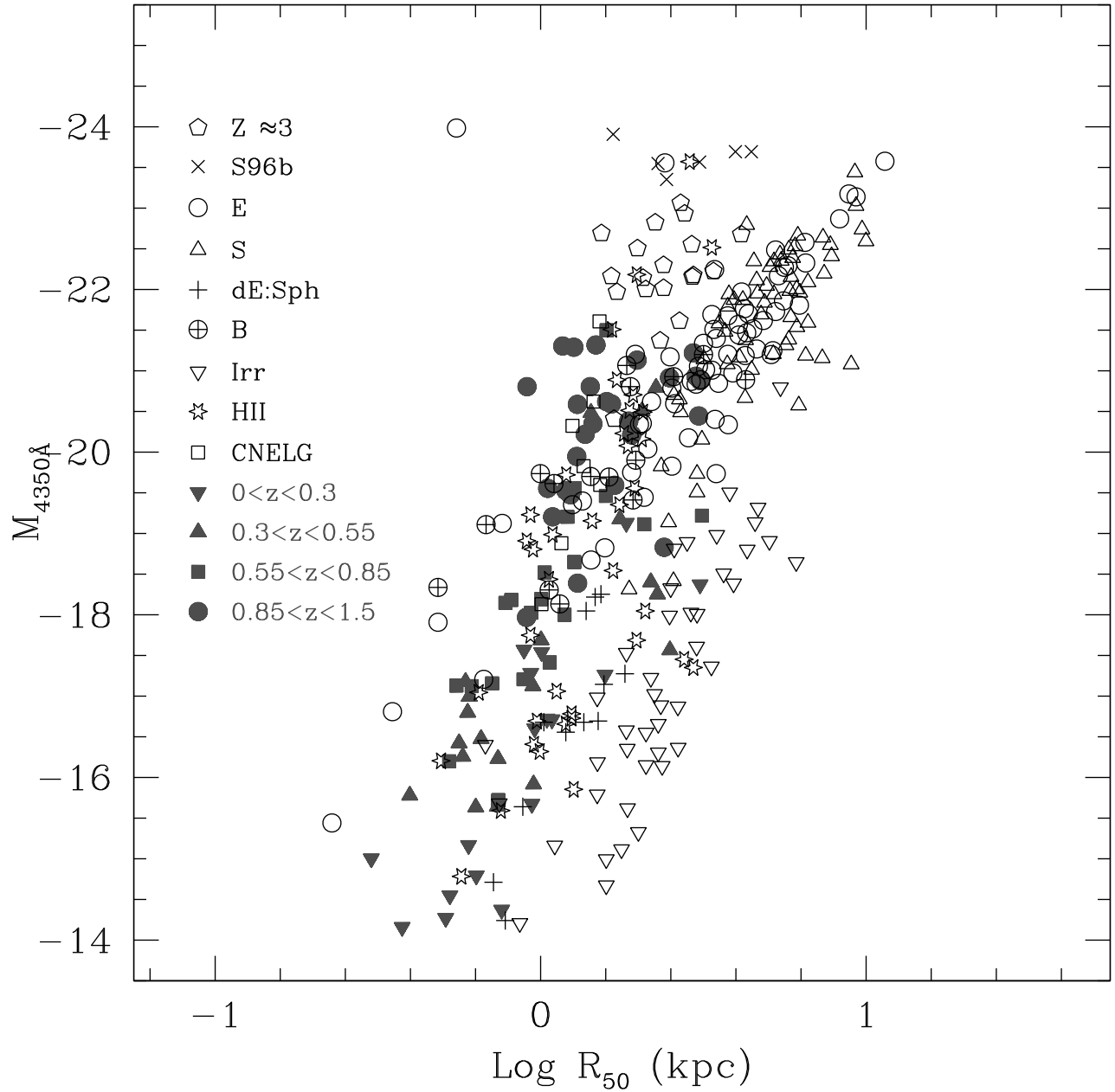


Fig. 11.— The size and luminosity of eGRAPES (solid symbols). This Figure is similar to Figure 7 in Lowenthal et al. (1997), accounting for our choice of h_{70} . The open symbols are for local ellipticals, dwarfs, ellipticals/spheroidal, spiral bulges, spirals, irregulars, HII galaxies, CNELGs, as well as the $z \approx 3$ HDF objects identified by Lowenthal et al. (1997).

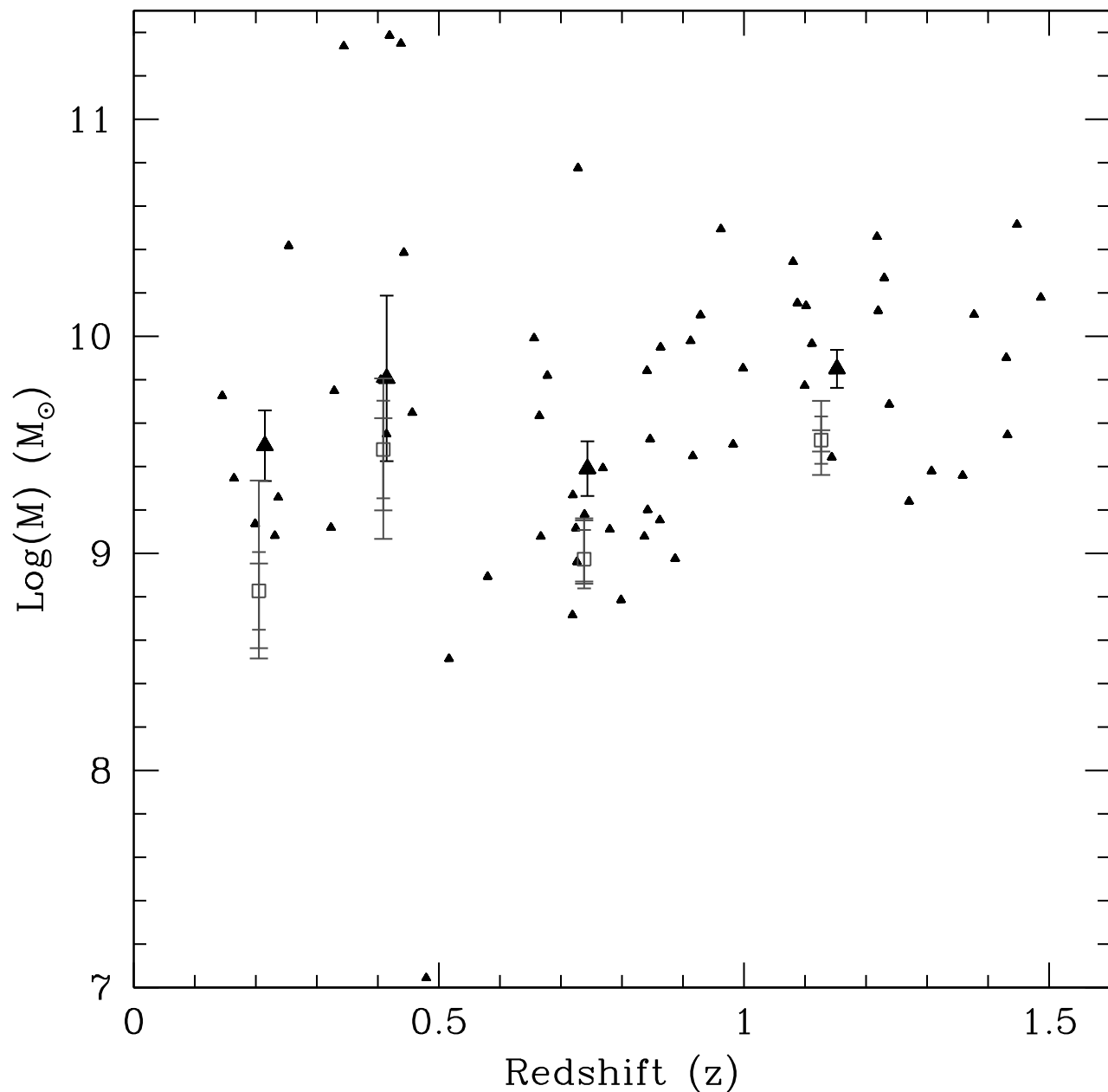


Fig. 12.— Masses of eGRAPES with $M_{B_{435}} \leq -17.5$. The average masses are indicated in the redshift bins of $z = 0.20, 0.41, 0.73, 1.15$ using error bars. Photometric masses, as well as the three SED derived mass estimates (error bars with open symbols) described in Section 7 are plotted. The filled triangles are the individual eGRAPES photometric mass estimates. The error bars show the 95% confidence limit, computed using bootstrapping.

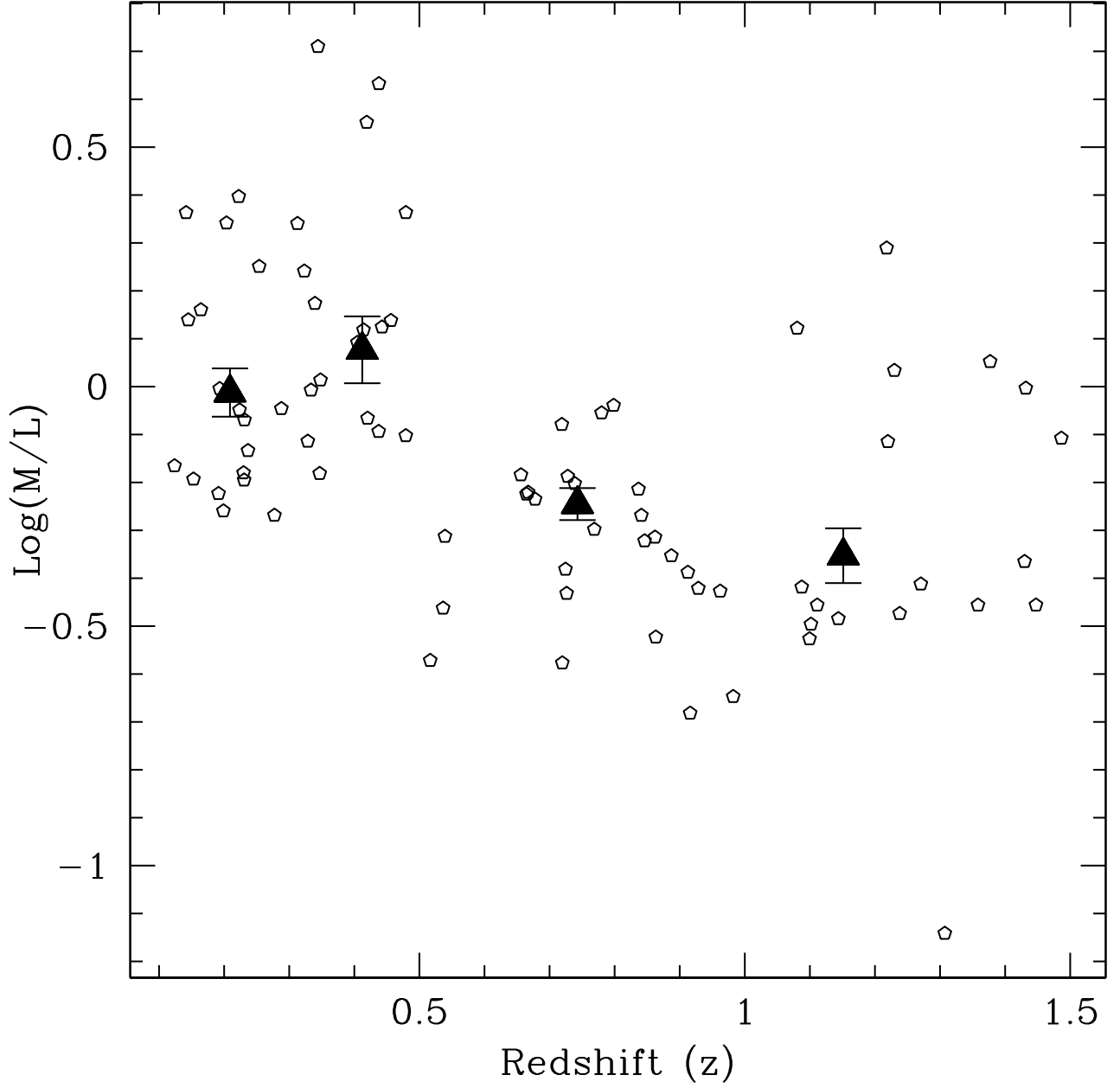


Fig. 13.— Mass-to-light ratio of eGRAPES with $M_{B_{435}} \leq -17.5$ (open pentagons). The average mass-to-light ratios are indicated in the redshift bins of $z = 0.20, 0.41, 0.73, 1.15$ using solid triangles and error bars. The error bars show the 95% confidence limit, computed using bootstrapping.

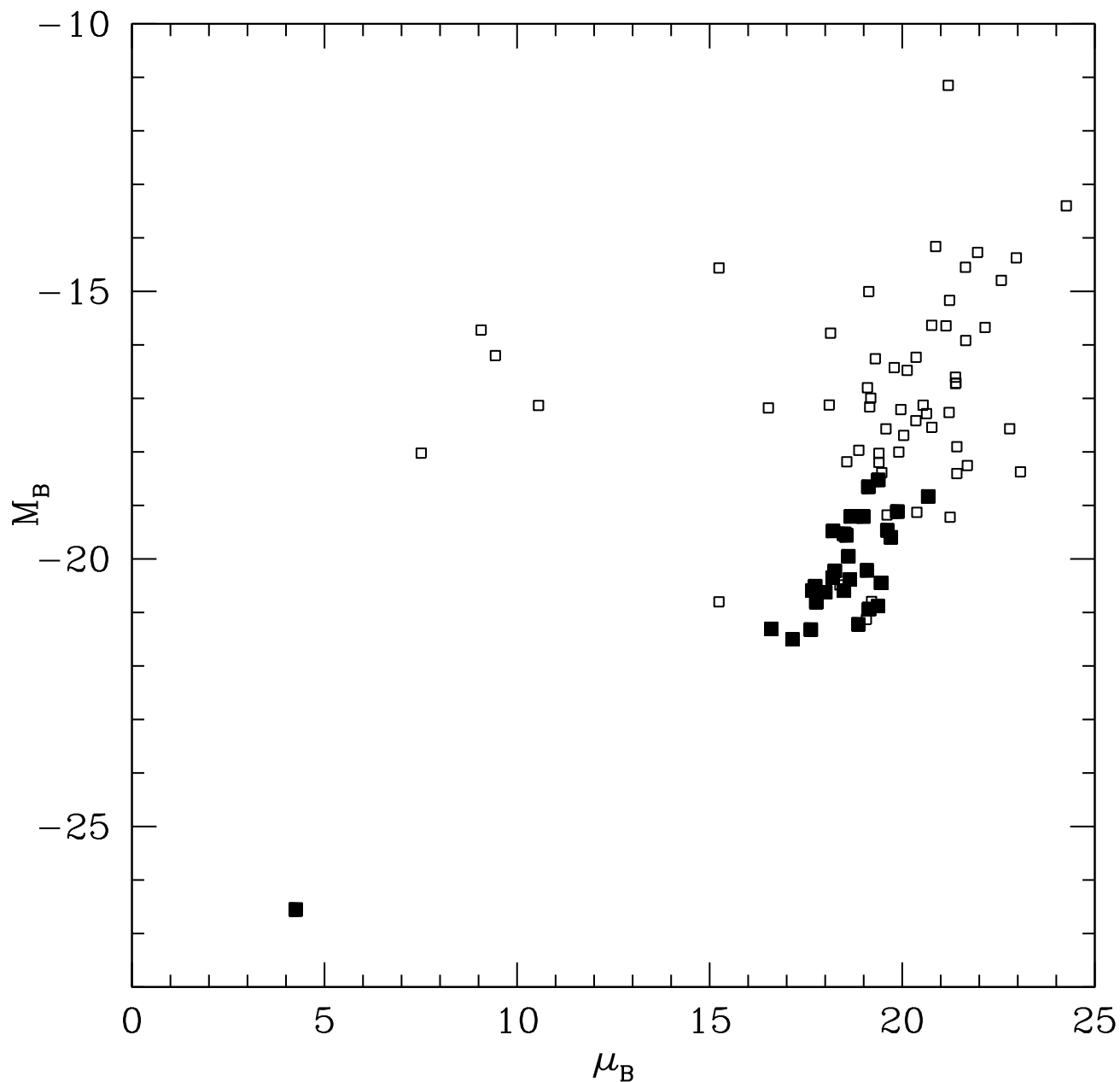


Fig. 14.— eGRAPES in an absolute rest-frame $M_{B_{435}}$ magnitude versus rest-frame B_{435} band surface brightness plot. eGRAPES objects are shown using open squares. eGRAPES luminous compact blue galaxies (LCBGs) candidates, as selected following the criteria from Werk et al. (2004), are shown using solid squares. The very bright objects at $M_B < -25$ is a quasar, while the four objects with $\mu_B \leq 12$ are relatively faint, unobscured (Type 1) AGNs.

REFERENCES

- Barden, M., et al. 2005, ArXiv Astrophysics e-prints, astro-ph/0502416
- Beckwith S., et al. 2005, in preparation
- Bell, E. F., McIntosh, D. H., Katz, N., & Weinberg, M. D. 2003, ApJS, 149, 289
- Bershady, M. A., Jangren, A., & Conselice, C. J. 2000, AJ, 119, 2645
- Bertin, E., & Arnouts, S. 1996, A&AS, 117, 393
- Bruzual, G., & Charlot, S. 2003, MNRAS, 344, 1000
- Charlot, S., & Fall, S. M. 2000, ApJ, 539, 718
- Conselice, C. J., Bershady, M. A., & Jangren, A. 2000, ApJ, 529, 886
- Conselice, C. J. 2003, ApJS, 147, 1
- Eke, V., Efstathiou, G., & Wright, L. 2000, MNRAS, 315, L18
- Fall, S. M., & Efstathiou, G. 1980, MNRAS, 193, 189
- Ferreras, I., & Silk, J. 2000, ApJ, 541, L37
- Ferguson, H. C., et al. 2004, ApJ, 600, L107
- Frei, Z., Guhathakurta, P., Gunn, J. E., & Tyson, J. A. 1996, AJ, 111, 174
- Fukugita, M., Shimasaku, K., & Ichikawa, T. 1995, PASP, 107, 945
- Garland, C. A., Pisano, D. J., Williams, J. P., Guzmán, R., & Castander, F. J. 2004, ApJ, 615, 689
- Garland, C. A., Williams, J. P., Pisano, D. J., Guzmán, R., Castander, F. J., & Brinkmann, J. 2005, ApJ, 624, 714
- Guzman, R., Koo, D. C., Faber, S. M., Illingworth, G. D., Takamiya, M., Kron, R. G., & Bershady, M. A. 1996, ApJ, 460, L5
- Guzman, R., Gallego, J., Koo, D. C., Phillips, A. C., Lowenthal, J. D., Faber, S. M., Illingworth, G. D., & Vogt, N. P. 1997, ApJ, 489, 559
- Guzman, R., Jangren, A., Koo, D. C., Bershady, M. A., & Simard, L. 1998, ApJ, 495, L13

- Guzmán, R., Östlin, G., Kunth, D., Bershady, M. A., Koo, D. C., & Pahre, M. A. 2003, *ApJ*, 586, L45
- Jangreen et al. 2005, in preparation
- Kent, S. M. 1984, *ApJS*, 56, 105
- Koekemoer, A. M., et al. 2004, *ApJ*, 600, L123
- Koo, D. C., Bershady, M. A., Wirth, G. D., Stanford, S. A., & Majewski, S. R. 1994, *ApJ*, 427, L9
- Koo, D. C., Guzman, R., Faber, S. M., Illingworth, G. D., Bershady, M. A., Kron, R. G., & Takamiya, M. 1995, *ApJ*, 440, L49
- Lauger, S., Burgarella, D., & Buat, V. 2004, *ArXiv Astrophysics e-prints*, astro-ph/0410355
- Lowenthal, J. D., et al. 1997, *ApJ*, 481, 673
- Malhotra, S., et al. 2005, *ArXiv Astrophysics e-prints*, astro-ph/0501478
- Marleau, F. R., & Simard, L. 1998, *ApJ*, 507, 585
- Mobasher et al., in preparation
- Pasquali et al., in preparation
- Peng, C. Y., Ho, L. C., Impey, C. D., & Rix, H. 2002, *AJ*, 124, 266
- Phillips, A. C., Guzman, R., Gallego, J., Koo, D. C., Lowenthal, J. D., Vogt, N. P., Faber, S. M., & Illingworth, G. D. 1997, *ApJ*, 489, 543
- Pirzkal, N., et al. 2004, *ApJS*, 154, 501
- Pirzkal, N., et al. 2005, *ApJ*, 622, 319
- Ravindranath, S., et al. 2004, *ApJ*, 604, L9
- Rix, H., et al. 2004, *ApJS*, 152, 163
- Rhoads, J. E. et al. 2005
- Schade, D., Lilly, S. J., Crampton, D., Hammer, F., Le Fevre, O., & Tresse, L. 1995, *ApJ*, 451, L1
- Schade, D., Lilly, S. J., Le Fevre, O., Hammer, F., & Crampton, D. 1996, *ApJ*, 464, 79

Sérsic, J.-L., 1968, Atlas de Galaxias Australes (Cordoba: Obs. Astron.)

Steidel, C. C., Adelberger, K. L., Giavalisco, M., Dickinson, M., & Pettini, M. 1999, ApJ, 519, 1

Thompson, R. I., et al. 2005, ArXiv Astrophysics e-prints, arXiv:astro-ph/0503504

Trujillo, I., et al. 2004, ApJ, 604, 521

Werk, J. K., Jangren, A., & Salzer, J. J. 2004, ApJ, 617, 1004

Xu, C. et al. 2005